Geophysical Research Letters

RESEARCH LETTER
10.1029/2024GL114460

Autogenic Curvature of Transgressive Shelf Profiles

Junhui Wang[1,2] and Tetsuji Muto[3]

[1]State Key Laboratory of Petroleum Resources and Engineering, China University of Petroleum (Beijing), Beijing, China, [2]College of Geosciences, China University of Petroleum (Beijing), Beijing, China, [3]Department of Environmental Science, Nagasaki University, Nagasaki, Japan

Key Points:

- During transgression, deltaic sedimentation cannot be sustained if the length of the downstream alluvial river exceeds the threshold
- The non-deltaic transgressive shelf steepens landward, reflecting autogenic shrinkage of the feeder alluvial system
- The governing equation for the shelf profile is supported by two-dimensional physical experiments and applications in natural systems

Supporting Information:

Supporting Information may be found in the online version of this article.

Correspondence to:

J. Wang and T. Muto,
wangjunhui@cup.edu.cn;
tmuto@nagasaki-u.ac.jp

Citation:

Wang, J., & Muto, T. (2025). Autogenic curvature of transgressive shelf profiles. *Geophysical Research Letters*, *52*, e2024GL114460. https://doi.org/10.1029/2024GL114460

Received 4 JAN 2025
Accepted 2 JUL 2025

Author Contributions:

Conceptualization: Junhui Wang, Tetsuji Muto
Formal analysis: Junhui Wang, Tetsuji Muto
Funding acquisition: Junhui Wang, Tetsuji Muto
Investigation: Junhui Wang, Tetsuji Muto
Methodology: Junhui Wang, Tetsuji Muto
Project administration: Junhui Wang, Tetsuji Muto
Software: Junhui Wang
Validation: Junhui Wang, Tetsuji Muto
Visualization: Junhui Wang, Tetsuji Muto
Writing – original draft: Junhui Wang
Writing – review & editing: Junhui Wang, Tetsuji Muto

Abstract Many continental shelves tend to steepen landward. Existing models attribute this curvature to a progressive attenuation of the effect of postglacial sea-level rise or sediment redistribution by modern coastal-marine processes. Here, we present an alternative framework in which shelf curvature arises from an inherent self-organizing mechanism. During sea-level rise, if the critical length of the downstream alluvial river is exceeded, deltaic sedimentation cannot be sustained. In this non-deltaic transgressive regime, the alluvial aggradation rate autogenically increases as the river shrinks, enhancing alluvial sediment accumulation and producing a steeper local shelf slope closer to the shoreline. Two-dimensional geometric modeling reveals a simple governing equation for the self-organized curvature of the shelf profile, with support from flume-tank experiments and applications to modern systems, providing a mechanistic basis for interpreting existing shelf profiles.

Plain Language Summary A shelf is the marginal zone of a continent that extends shallowly into the sea. Modern shelves are characterized by different shapes and sizes; they can be steep or gentle, wide or narrow, and control the physicochemical processes and thus the ecosystem of the shallow sea. Throughout Earth's history, shelves have been important geological interfaces that are repeatedly created and filled with sediment in response to sea-level rise and fall, thereby forming strata. A common feature of many shelves is that they have a concave upward profile that steepens in the landward direction. Such a curvature pattern is typically interpreted as the result of wave erosion or an increasing contribution of upstream sediment input. Here, we show that the landward steepening of the shelf is an autogenic behavior caused by an inherent mechanism. Owing to this inherent mechanism, the shelf has a theoretical profile that is determined by the terrestrial hinterland and alluvial slopes. Given similar background slope conditions, shelves differ in shape and scale because they develop at different stages corresponding to different segments along the theoretical curve. The autogenic landward-steepening mechanism provides a new interpretation of shelf genesis.

1. Introduction

A shelf is a highly productive and dynamic oceanic environment that supports diverse marine life owing to ample sunlight, oxygen, and nutrients (Nittrouer & Wright, 1994; Walsh, 1988); its profile is crucial, as it determines the local and global bathymetry. In geological history, the shelf profile is also a main factor in stratigraphic analyses, because it determines the basin-marginal strata stacking process (Catuneanu, 2019; Patruno & Helland-Hansen, 2018; Wang & Muto, 2021). Therefore, quantifying shelf profiles is fundamental for understanding the marine geomorphology and geology.

Many modern and ancient shelves exhibit landward-steepening curvatures (Anell, 2024a, 2024b; Fagherazzi & Overeem, 2007; Patruno et al., 2015). Two views exist regarding the origin of such curvatures: (a) a change in the accommodation/supply (A/S) ratio, such as a deceleration of sea-level rise and/or an increase in sediment input (Cattaneo & Steel, 2003) and (b) sediment excavation at the shoreface and re-deposition both offshore and onshore (Anell, 2024a, 2024b; Fagherazzi & Overeem, 2007; Iwasaki & Parker, 2020; Swift & Thorne, 1992). The former regards the shelf profile as a geological relic, whereas the latter perceives it as a product of the modern coastal-marine processes.

Here, we present an autogenic mechanism that generates curved shelf profiles. This can occur under the following conditions: (a) constant relative sea-level rise, (b) constant upstream sediment supply, and (c) no significant sediment reworking by marine processes. Through two-dimensional (2D) geometric modeling, we obtained a simple equation governing the shelf profile. Given the sediment supply rate, relative sea-level rise rate, and geometrical parameters, including the downstream alluvial and hinterland slopes, the shelf adjusts itself to

produce a theoretical profile. Each transgressive shelf has a theoretical profile, and significant deviations may indicate unsteady external forcing factors.

2. Theoretical Model

2.1. Non-Deltaic Transgression

Figure 1a shows an experimental shelf system created with steady forcing by constant sea-level rise and upstream sediment supply without wave reworking. The shelf steepened landward, and only the topset developed during the transgression (cf. accretionary transgression, Helland-Hansen & Hampson, 2009). This type of transgression is termed non-deltaic transgression, because the entire system lacks the foreset part and thus differs from a typical three-layer deltaic system (Muto & Wang, 2024; Tomer et al., 2011; Wang & Muto, 2021).

Non-deltaic transgression occurs inevitably when the downstream alluvial system exceeds its critical length (L_{crt}). Assuming linear profiles for both the hinterland and alluvial surfaces in the dip direction (Figure 1b), L_{crt} is derived from sediment mass conservation as follows (Tomer et al., 2011):

$$L_{crt} = \frac{\gamma\sqrt{1+\alpha^2}}{\gamma-\alpha}\Lambda_{2D}, \tag{1}$$

where α and γ are the alluvial and hinterland slopes, respectively (Figure 1a). Λ_{2D} is the autostratigraphic length scale in the 2D space (Muto, 2001), defined as follows:

$$\Lambda_{2D} = \frac{q_s}{|R_{sl}|}, \tag{2}$$

where q_s is the volumetric sediment supply rate per unit width, and R_{sl} is the rate of relative sea-level change ($R_{sl} > 0$ for rise). Any length quantity can be discussed in a dimensionless form by normalization with Λ_{2D}. For example, the dimensionless critical length L_{crt}^* ($=L_{crt}/\Lambda_{2D}$) is approximately equal to 1 if $\gamma >> \alpha$ (Equation 1; dimensionless entities are marked with an asterisk throughout this paper). Using this dimensionless approach, systems of different scales can be compared effectively.

In the experiment shown in Figure 1a, although the alluvial river shrank with time, its length (L) never became perceptibly smaller than L_{crt} ($L \geq L_{crt}$); thus, the non-deltaic transgression was sustained throughout the duration of experiment. During the transgression, the local shelf slope (ϕ_{local}) immediately basinward of the shoreline increased as the sea level rose (Figure 1b). This is because river shortening forces sediment accumulation into a smaller area, elevating the aggradation rate of the landward river. Specifically, the relationship between ϕ_{local} ($\alpha \leq \phi_{local} \leq \gamma$) and L can be expressed as follows:

$$\phi_{local} = \frac{\alpha L}{L - \Lambda_{2D}\sqrt{1+\alpha^2}} = \frac{\alpha L^*}{L^* - \sqrt{1+\alpha^2}}, \tag{3}$$

where L^* is the dimensionless form of L (see Text S1 in Supporting Information S1 for the derivation).

Figure 1c shows that when the alluvial river is extremely over-extended (i.e. $L^* >> 1$), ϕ_{local} approaches α. As L^*decreases, ϕ_{local} increases. Once the alluvial river shortens to the critical length ($L \sim L_{crt}$), further shortening triggers foreset formation and terminates the non-deltaic transgression. Consequently, ϕ_{local} is defined by the subaqueous foreset slope, β, which can be as large as the sediment repose angle (Anell, 2024a, 2024b; Tomer et al., 2011). This occurs in steep hinterland settings ($\gamma > \beta$; Wang & Muto, 2021). Conversely, when $\gamma < \beta$, non-deltaic transgression continues without further river shortening, that is, $L = L_{crt}$, with ϕ_{local} stabilizing at its maximum ($\phi_{local} \sim \gamma < \beta$) indefinitely (Wang & Muto, 2021; Figure 1a).

2.2. Governing Equation of the Non-Deltaic Transgressive Shelf Profile

In the x–z coordinate system, where the origin (0, 0) is the intersection of the hinterland basement and the horizontal line through the shelf-edge point (Figure 1b), Equation 3 can be expressed as follows (see Text S1 in Supporting Information S1 for the derivation):

10.1029/2024GL114460

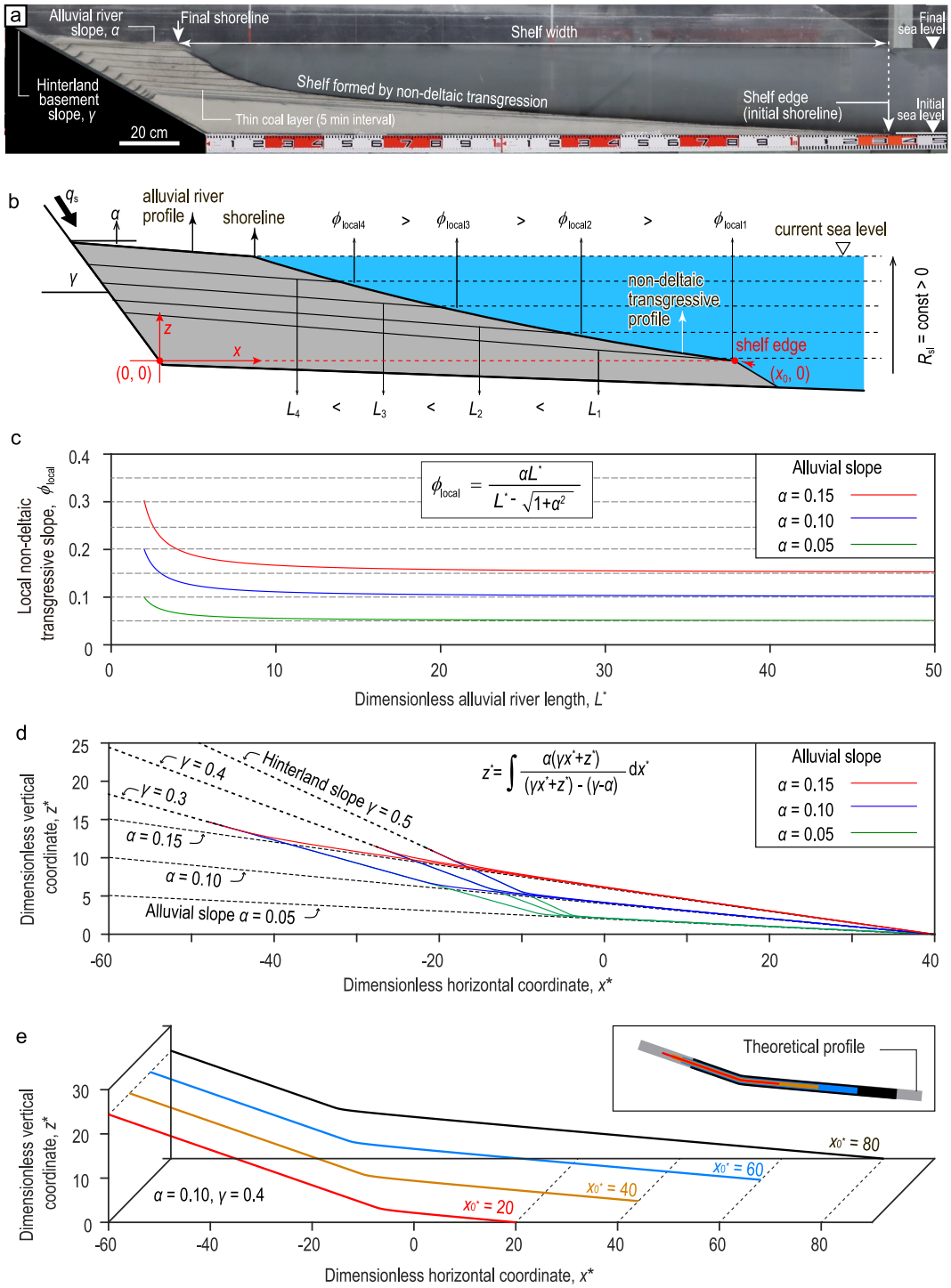

Figure 1. Illustration of the non-deltaic transgression. (a) A non-deltaic transgressive shelf produced in a two-dimensional flume. Experimental conditions: per unit width sediment supply rate $q_s = 0.342$ cm^2/s (concentration: 2.51%), rate of sea-level rise $R_{sl} = 0.00800$ cm/s, amplitude of sea-level rise $A_{sl} = 28.8$ cm, hinterland basement slope $\gamma = 0.577$, alluvial river slope $\alpha = 0.0612$, critical alluvial length $L_{crt} = 47.9$ cm (Equation 1), initial alluvial length $L_0 = 250$ cm, and final alluvial length $L_{final} = 47.8$ cm ~ L_{crt}. The sediment was uniform quartz sand (0.2 mm). (b) Schematic diagram of a landward steepening shelf profile developed during non-deltaic transgression associated with the shortening of the feeding alluvial river (length L). (c) Relationship between local shelf slope (ϕ_{local}) and dimensionless alluvial length (L^*). Simulated using Equation 3 and different α values. (d) Simulated non-deltaic shelf profiles showing that ϕ_{local} approaches α basinward and γ landward. Simulated using Equation 5b. (e) Simulated non-deltaic shelf profiles with different initial alluvial river lengths (L_0^*; reflected by different x_0^* values) and fixed A_{sl}^*, α, and γ. The inset shows that the four profiles match different segments of a single theoretical curve.

$$\phi_{\text{local}} = \frac{\alpha(\gamma x + z)}{(\gamma x + z) - \Lambda_{2D}(\gamma - \alpha)} = \frac{\alpha(\gamma x^* + z^*)}{(\gamma x^* + z^*) - (\gamma - \alpha)}, \tag{4}$$

where x^* and z^* are the dimensionless forms of x and z, respectively.

Theoretically, ϕ_{local} represents the tangent of the local shelf profile. Integrating Equation 4 with respect to x yields the governing equation for the non-deltaic shelf profile (z_{shelf}; see Text S1 in Supporting Information S1 for the derivation):

$$z_{\text{shelf}} = \int_{(x_0,0)}^{(x_1,z_1)} \frac{\alpha(\gamma x + z)}{(\gamma x + z) - \Lambda_{2D}(\gamma - \alpha)} dx, \tag{5a}$$

$${z_{\text{shelf}}}^* = \frac{z_{\text{shelf}}}{\Lambda_{2D}} = \int_{({x_0}^*,0)}^{({x_1}^*,{z_1}^*)} \frac{\alpha(\gamma x^* + z^*)}{(\gamma x^* + z^*) - (\gamma - \alpha)} dx^*, \tag{5b}$$

where ${z_{\text{shelf}}}^*$ is the dimensionless form of z_{shelf}, and $({x_0}^*, 0)$ and $({x_1}^*, {z_1}^*)$ are the dimensionless forms of the initial and final shoreline positions $(x_0, 0)$ and (x_1, z_1), respectively. Specifically, at the initial shoreline, the following apply:

$$x_0 = \frac{L_0(\gamma - \alpha)}{\gamma\sqrt{1 + \alpha^2}}, \tag{6a}$$

$${x_0}^* = \frac{x_0}{\Lambda_{2D}} = \frac{{L_0}^*(\gamma - \alpha)}{\gamma\sqrt{1 + \alpha^2}}, \tag{6b}$$

where ${L_0}^*$ is the dimensionless form of the initial alluvial length (L_0) before transgression.

Figure 1d illustrates simulated shelf profiles with different combinations of α and γ values from Equation 5b. Evidently, (a) shelf profiles vary systematically with α and/or γ values, (b) ϕ_{local} approaches α in the distal seaward direction and γ in the landward direction; and (c) smaller α and/or larger γ benefits an earlier (i.e., smaller z^*) approaching of ϕ_{local} to γ during the transgression.

We note that Equation 5a is derived from the geometric model (Figure 1b), regardless of whether the model is at the laboratory or natural scale. The significant disparity in scale between the laboratory and natural models is mainly due to the differences in the magnitudes of sediment supply and sea-level change, which in turn affect the length scale Λ_{2D}. Normalized with corresponding Λ_{2D}, laboratory and natural models can be compared within a unified x^*–z^* space, although the slope parameters (i.e., α, γ) are also crucial. This implies that given a specific scale and geometric parameters, Equation 5b applies to any non-deltaic transgressive systems.

2.3. Mature Shelf

In Figure 1d, both the shelf slope and alluvial length remain constant during the final stage of the non-deltaic transgression ($\phi_{\text{local}} \sim \gamma$; $L = L_{\text{crt}}$). Such a steady state can be regarded as a mature phase of shelf development, because there is no further change in strata stacking and landform evolution (Muto & Wang, 2024; Wang & Muto, 2024; Wu et al., 2020). As the shelf approaches maturity, it steepens.

The proximity of a specific shelf to the mature stage depends on the amplitude of the sea-level rise (A_{sl}, reflected by z).

$${A_{\text{sl}}}^* = \frac{A_{\text{sl}}}{\Lambda_{2D}} = \frac{A_{\text{sl}}|R_{\text{sl}}|}{q_s} = z^*, \tag{7}$$

where ${A_{\text{sl}}}^*$ is the dimensionless form of A_{sl}. Equation 7 indicates that for a particular alluvial system (q_s = const), a larger amplitude and/or rate of relative sea-level rise yields a larger ${A_{\text{sl}}}^*$ (z^*). With a larger ${A_{\text{sl}}}^*$, the alluvial river

is shortened more effectively, and the shelf profile is curved more effectively. Given sufficiently large A_{sl}*, the slope condition $\phi_{local} \sim \gamma$ is realized for any over-extended alluvial rivers undergoing relative sea-level rise.

Figure 1d shows the theoretical shelf profiles starting at x_0* = 40. In various alluvial-shelf systems, the x_0* value, which reflects the initial alluvial river length before transgression (Equation 6b), is seldom the same. For systems with fixed α and γ and different x_0* values, less over-extended alluvial rivers (i.e., smaller x_0* value) lead to faster attainment of the mature shelf stage (smaller z* value), as shown in Figure 1e. The difference is that these profiles correspond to different segments of the full theoretical curve, implying that they evolve at different stages of a virtually full shelf development process.

The above analyses indicate that the sea-level rise amplitude (A_{sl}*) and initial alluvial river length (L_0*, representative of x_0*) define the landward and seaward limits of the shelf, respectively. Different pairs of A_{sl}* and L_0* (or x_0*) values indicate distinct shelf profiles that correspond to specific segments of a theoretical curve. A larger L_0* (or x_0*) and smaller A_{sl}* indicate a more seaward segment on the theoretical curve, creating a gentler and flatter shelf. Conversely, a smaller L_0* ($>L_{crt}$*) and larger A_{sl}* produce steeper and more curved shelves closer to maturity (Figure 1d).

3. Two-Dimensional Flume-Tank Experiments

3.1. Design

The proposed model was tested through a series of 2D flume-tank experiments. The floor of the flume (2.0 cm wide, 56.7 cm deep, and 3.0 m long) consists of a horizontal section that serves as the initial basin floor, and a 31°-inclination upstream section that serves as the hinterland slope (i.e., $\gamma \sim 0.612$) (Figure S2 in Supporting Information S1). During the experiment, sea level cycled with symmetric rise and fall at constant rates and periods. Sediment and water were supplied from the upstream end of the flume at fixed discharge values. For the present arguments, the focus was placed on the rising half-cycles during which non-deltaic transgression occurred.

Three run series were conducted with different sea-level amplitudes (A_{sl}), that is, high (H_A; 46.1–47.9 cm), medium (M_A; 23.1–23.4 cm), and low (L_A; 11.4–11.5 cm). Each A_{sl}-modulation series included three runs with different $|R_{sl}|$ values, that is, high (H_R; 12.8–12.9 × 10^{-3} cm/s), medium (M_R; 8.54–8.62 × 10^{-3} cm/s), and low (L_R; 4.25–4.33 × 10^{-3} cm/s). During each run, A_{sl} and $|R_{sl}|$ were kept constant (sea-level curves in Figure S3 in Supporting Information S1). Except for A_{sl} and $|R_{sl}|$, consistent experimental conditions were maintained across all runs, including sediment material (uniform 0.2 mm natural quartz sand), sediment supply rate (q_s = 0.134–0.160 cm^2/s), and water supply rate (q_w = 2.18–2.30 cm^2/s) (Table S1 in Supporting Information S1). Owing to differences in sea-level cycling periods (half-period $T_{sl} = A_{sl}/|R_{sl}|$), sea levels underwent varying numbers of cycles in different runs (Figures S4–S12 in Supporting Information S1).

Each run was initiated at time 0 with a 1.0-cm basin water depth and no preexisting sediments. Non-deltaic transgression occurred during the rising half-cycles, when the alluvial river length exceeded the critical value ($L > L_{crt}$). The initial alluvial length (L_0) recorded before each sea-level rise increased progressively across cycles. Digital photographs were captured every 60 or 30 s to document the experiments. The average alluvial slope, α, was measured from each photograph directly. All length-scale quantities were normalized by dividing by Λ_{2D} (Equation 2).

3.2. Results

As the cycles continued, the depositional wedge grew, and the initial alluvial river lengthened before each transgression. Non-deltaic transgression commenced from cycle 2 in all runs. Figures S4–S12 in Supporting Information S1 show that each resulting shelf matched the theoretical predictions. For all runs, the curvature of the shelf profiles in earlier cycles was sharper than that in later cycles (Figure 2a). Once the system sufficiently extended in later cycles, the overall shelf profile was gentler and closer to a linear pattern, with an average slope (ϕ_{avg}, from shelf edge to shoreline) approaching α (Figure 2a). This α value remained nearly constant across all runs ($\alpha \sim 0.13 \pm 0.03$).

The shelf curvature is strongly correlated with the sea-level rise amplitude (A_{sl}*), which varies among runs as it is modulated by different combinations of A_{sl} and R_{sl} (Equation 7). Figure 2; Figures S4–S12 in Supporting Information S1 show that runs with larger A_{sl}* (larger A_{sl} and/or $|R_{sl}|$) produced shorter alluvial rivers and steeper

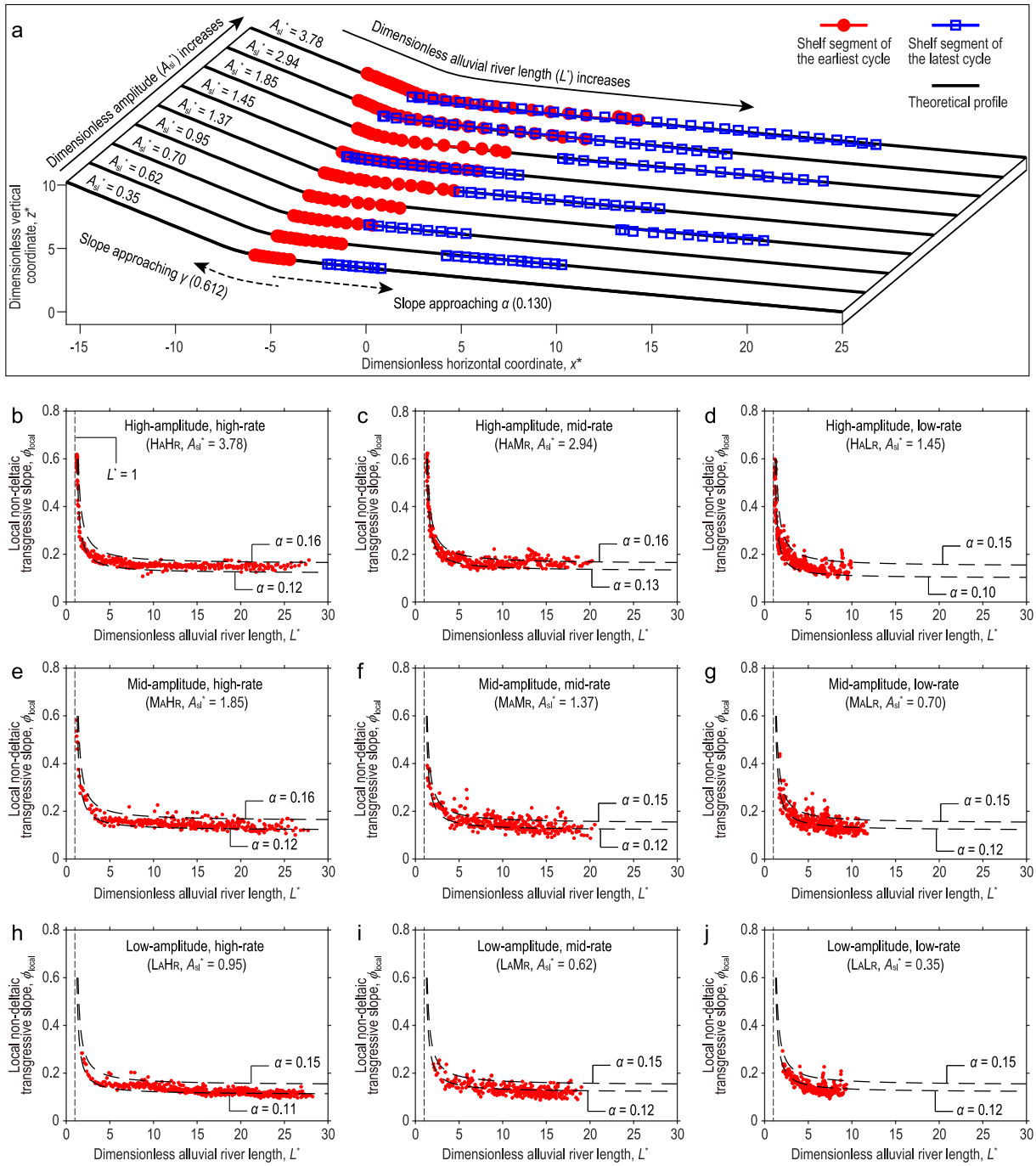

Figure 2. Shelves generated with different amplitudes (A_{sl}*) and initial alluvial lengths (L_0*) in the experiment. Data are compared in dimensionless space by normalizing all length quantities with the autostratigraphic length scale (Λ_{2D}). We note that Λ_{2D} varied across runs due to different $|R_{sl}|$ values. (a) Comparison of experimental and theoretical shelf profiles. Shelves from all runs share a uniform theoretical profile because of equaling hinterland ($\gamma \sim 0.612$) and alluvial slopes ($\alpha \sim 0.130$). Profiles from the earliest (cycle 2) and latest cycles are presented; intermediate-cycle segments lie between these extremes (Figures S4–S12 in Supporting Information S1). The theoretical curve is modeled based on Equation 5b with $\alpha = 0.130$ and $\gamma = 0.612$. (b–j) Relationship between ϕ_{local} and L^* for each of the nine runs. The plots align with the curves derived from Equation 3, using the maximum and minimum α values obtained from each run. In panels b–f, shelf maturity is indicated by $\phi_{local} \sim \gamma$ and $L^* \sim 1$.

shelves. For example, in earlier cycles of the H_AH_R, H_AM_R, M_AH_R, H_AL_R, and M_AM_R runs, where A_{sl}* values were relatively large, ϕ_{local} reached the theoretical limit (approximately γ) and the dimensionless alluvial length approximated 1 ($L^* \sim L_{crt}^* \sim 1$) (Figures 2b–2f).

All runs experienced the transition from the early steep-shelf stage to the late gentle-shelf stage. This is because the alluvial length before each transgression (L_0*) controls also the shape of the shelves. For each run (with A_{sl}* being constant), the shelf profile tended to curve more sharply in earlier cycles when L_0* was smaller (Figure 2a). In later cycles, when the system had greatly expanded (L_0* >> L_{crt}*), the shelf became gentler and linear, with an average slope approaching that of the alluvial river (α) (Figures 2a and 3a).

Additionally, the transition from the earlier steep stage to the later gentle stage in simulations with larger A_{sl}* values was slower than that in simulations with smaller A_{sl}* values, as a larger A_{sl}* value has a stronger effect on shelf steepening. In runs with relatively small A_{sl}* values (i.e., excluding runs H_AH_R (A_{sl}* = 3.78), H_AM_R (A_{sl}* = 2.94), and M_AH_R (A_{sl}* = 1.85)), most shelves showed a gentle and linear pattern (Figure 3a; Figures S4−S12 in Supporting Information S1). This occurred because in these low-A_{sl}* runs, the transition from the early to the late stage was completed after only two or three sea-level cycles.

In each run, the shelf becoming gentler in later cycles also meant that it became wider (width, W; horizontal length from the shoreline to the shelf edge; Figure 1a). This is because, given the same A_{sl}*, the average slope (ϕ_{avg}) and width (W) of the shelf are inversely correlated (Figure 3b):

$$\phi_{avg} = \frac{A_{sl}}{W} = \frac{A_{sl}^*}{W^*}, \tag{8}$$

where W* is the dimensionless form of W. Equation 8 indicates that, under a similar transgressive background (same A_{sl}*), wider shelves are always gentler.

4. Application to Natural Modern Systems

4.1. General Tendency of Modern Major Shelves

Modern shelves (Holocene flooding surfaces) created by postglacial transgression (21–8 ka) were often accompanied by the recession of sediment delivery systems (Helland-Hansen et al., 2012; Wang et al., 2019), and many were fed by far over-extended alluvial rivers (i.e., L_0* >> L_{crt}*) before the onset of the transgression (Muto & Wang, 2024; Tomer et al., 2011; Törnqvist et al., 2006). The A_{sl}* and L_0* values are different for alluvial-shelf systems with different Λ_{2D} values (Table S2 in Supporting Information S1). Equation 8 implies that fixing any one of the three parameters ϕ_{avg}, A_{sl}* or W* imposes deterministic relationships on the remaining two. As shown in Figure 3c, shelves with similar A_{sl}* values display a reciprocal relationship between width (W*) and slope (ϕ_{avg}): wider shelves correlate with gentler slopes. This is because the steeper (or narrower) shelves under comparable A_{sl}* evolve closer to their intrinsic mature state (Figures S13–S16 in Supporting Information S1). Therefore, each Holocene alluvial-shelf system responded uniquely to the postglacial sea-level rise through specific A_{sl}* and L_0*combinations, consistent with the theoretical framework presented here.

4.2. Rio de Janeiro Shelf

The shelf system off Rio de Janeiro State of Brazil, systematically measured using seismic line data, serves as an ideal natural example for testing the model (Figure 4). The current Rio de Janeiro shelf was developed by postglacial transgression following the landward retreat of the strand plain, which effectively fed sediment to the shelf. Existing seismic stratigraphic analyses (Reis et al., 2013) have confirmed that the Holocene transgression was non-deltaic (Figures 4c and 4d). Bathymetric data from the southwest to northeast show that the shelf has a curvature with landward steepening (Figure 4a).

We compiled existing data to explain this phenomenon using this model. The postglacial transgression caused a relative sea-level rise of ∼120 m (A_{sl}) over ∼12 kyr (Reis et al., 2013; Figure 4b), yielding an R_{sl} of 10 m/kyr. Maia et al. (2010) reported two shore-perpendicular cross-sections that showed stratigraphic architectures over the past 500 kyr (sections (A) and (B); Figures 4c and 4d). By dividing the depositional area by 500 kyr, the q_s values along sections (A) and (B) were calculated as 1.7×10^4 and 2.4×10^4 m^2/kyr, respectively. The length scale Λ_{2D} was then calculated at 1,700 and 2,400 m for sections (A) and (B), respectively.

By normalizing the real-world shelf profile with Λ_{2D}, the two sections fit a particular segment of the theoretical profile (Figures 4e and 4f). After normalization, A_{sl}* values were calculated at 0.07 and 0.05 in sections (A) and (B), respectively, that is, a larger A_{sl}* corresponds to a steeper shelf profile. In addition, the initial alluvial length

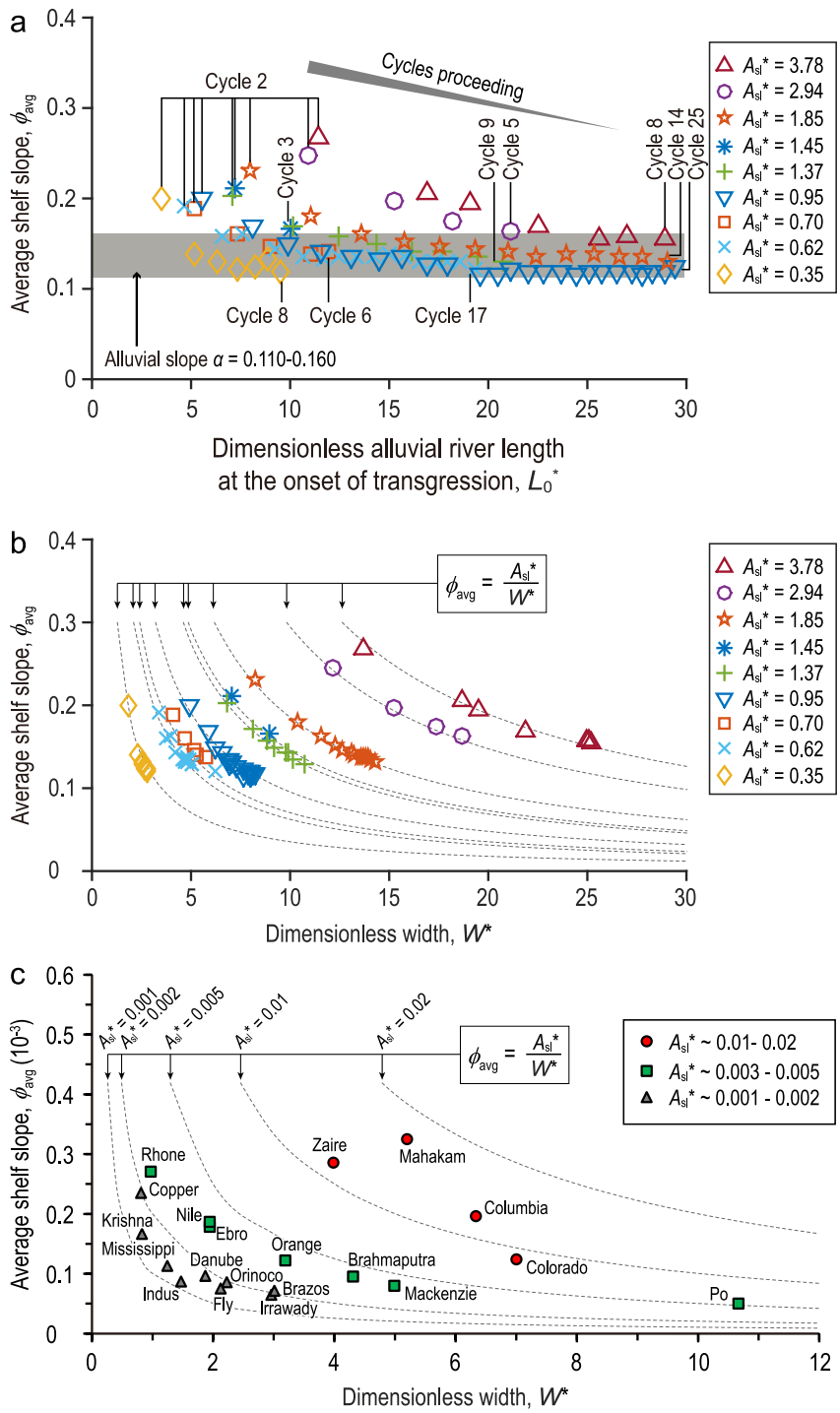

Figure 3. Relationships among the average shelf slope (ϕ_{avg}), initial alluvial river length (L_0), amplitude of sea-level rise (A_{sl}), and shelf width (W). (a) Relationship between ϕ_{avg} and L_0*, documented from the nine experimental runs. (b) Reciprocal relationship between ϕ_{avg} and W* (dimensionless) at maximum transgressions (Figures S4–S12 in Supporting Information S1). (c) Plots of ϕ_{avg} versus W* of modern shelves fed by major rivers globally. Data from Burgess and Hovius (1998) and the Global Multi-Resolution Topography data set of Ryan et al. (2009). See these natural shelf profiles, which are grouped by A_{sl}*, in Figures S13–S16 in Supporting Information S1.

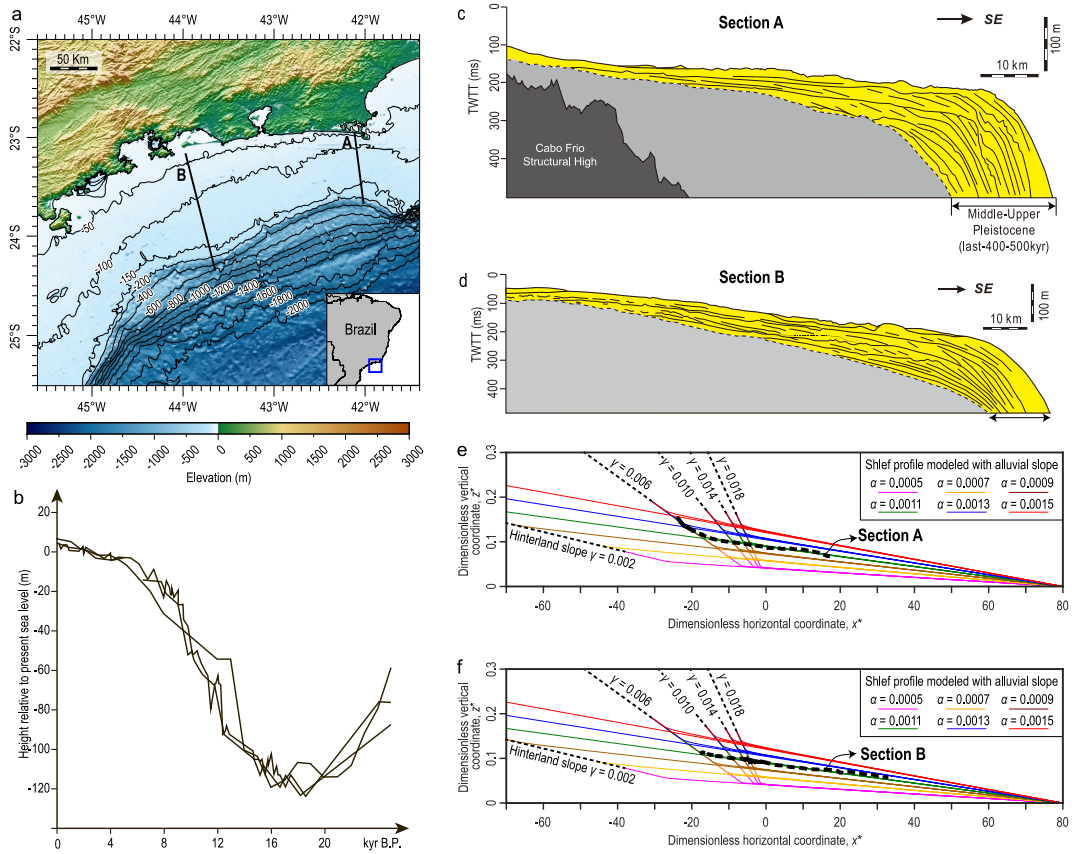

Figure 4. Model application to the modern Rio de Janeiro shelf. (a) Terrain map of the Rio de Janeiro shelf, which decreases in width (shoreline to shelf edge) from west to east. Data from SRTM15+ (Tozer et al., 2019). (b) Sea-level curves since 25 ka (Reis et al., 2013). (c–d) Pleistocene successions of sections (A) and (B), respectively (Maia et al., 2010). (e–f) Dimensionless shelf profiles (A–B) compared with modeled profiles that adopted different combinations of α and γ values. Both profiles align with a specific segment of the theoretical curve modeled with $\alpha = 0.0011$ and $\gamma = 0.006$. Profile data (A–B) from Reis et al. (2013).

(L_0*) decreased from southwest to northeast (Figures 4e and 4f). While decelerating sea-level rise over the past 5–6 kyr likely drove landward shelf steepening (Figure 4b), the combination of a larger A_{sl}* and smaller L_0* is highlighted as a non-negligible factor in shaping the present Rio de Janeiro shelf system, which steepens toward section (A).

4.3. Implications

For non-deltaic transgressive shelves, a theoretical profile exists when external forcing factors are constant. Deviations from this theoretical curve indicate changes in these factors. Consider a shelf divided into segments and each shows a landward-steepening pattern (Figure S17a in Supporting Information S1). This implies that the Λ_{2D} value of a given segment is smaller and the L_0* is larger than the respective value of the seaward segment. A likely cause is that the relative sea-level rise had multiple episodes of acceleration and/or the sediment supply had multiple episodes of decreasing. When foresets downlap on the landward part of the shelf (Figure S17b in Supporting Information S1), a probable reason is that the deceleration of the relative sea-level rise and/or increases in sediment supply result in a larger Λ_{2D} value (i.e., much larger than the alluvial length before foreset formation; $L_0^* < \Lambda_{2D}$).

We hypothesize that not all external forcing variations are readily detectable. As shown in Figures 1c and 1d, shelf profiles change slowly with x* when the shelf is far away from maturity, that is, under large L* conditions, $|dz^*/dx^*|$ is minimal ($\sim\alpha$). This implies that the external forcing changes that cause variations in L* may not be distinctly registered on the shelf profiles. Conversely, forcing variations are more likely to be recorded when

$|dz^*/dx^*|$ is pronounced. Specifically, $L^* \leq 5$ appears to be a reasonable range for profile sensitivity, as $|dz^*/dx^*|$ significantly increases here (Figures 1c and 2b–2j). Thus, if $L^* \leq 5$ is realized either before or after the variations of external forcing factors, these variations are more likely to leave detectable signatures on the shelf geometry.

The concept here is based on a 2D model. In a three-dimensional (3D) consideration, Muto and Wang (2024) indicates that non-deltaic transgression occurs in two sequential stages. In the first stage, the alluvial river retreats steadily, with sediment deposition being limited along its path. In the second stage, after substantial shrinkage of the alluvial surface, the alluvial river migrates quickly along the entire shoreline, causing the shelf to steepen uniformly along the shoreface. Uneven sediment distribution in the early transgression and even distribution in the later transgression result in varied shelf profiles across different dip directions. Shelf profiles crossing the former alluvial river path show a more gradual landward curvature than those away from the ancient alluvial river course.

5. Conclusions

The non-deltaic transgressive system, fed by the far over-extended alluvial river, inherently produces landward-steepening shelf profile curvatures accompanied by progressive river shortening. This can occur even with steady external forcing and is therefore an inherent behavior. A critical implication of the model is that natural shelves exhibiting different curvatures may simply reflect different stages of the evolution characterized by different magnitudes of autostratigraphic length scale Λ_{2D} and initial alluvial length. Alternatively, these shelves may represent different segments of the same theoretical profile. Thus, significant deviations from the baseline theoretical profile reflect unsteady forcing factors.

Conflict of Interest

The authors declare no conflicts of interest relevant to this study.

Data Availability Statement

Experimental data sets and databases of natural alluvial-delta-shelf systems for this research can be accessed at Zenodo repository (Wang & Muto, 2025). Data set of the SRTM15+ is available in the figshare repository (Tozer & Sandwell, 2019).

Acknowledgments
This study was jointly supported by the National Natural Science Foundation of China (42172108), the Institute of Geology and Geophysics of the CAS (THEMSIE04010101), and a Japanese Grant-in-Aid for Scientific Research (23K03509). We thank Wei Zhang and Gesi Tao for their help in conducting supplementary experiments. We are grateful to Ingrid Anell, Austin Chadwick and another anonymous reviewer for their constructive comments and suggestions and Neil Ganju for handling the manuscript.

References

Anell, I. (2024a). The fourth slope: A fundamental new classification of continental margins. *Basin Research*, *36*(2), e12863. https://doi.org/10.1111/bre.12863

Anell, I. (2024b). The quintessential s-shape in sedimentology: A review on the formation and controls of clinoform shape. *Earth-Science Reviews*, *254*, 104821. https://doi.org/10.1016/j.earscirev.2024.104821

Burgess, P. M., & Hovius, N. (1998). Rates of delta progradation during highstands: Consequences for timing of deposition in deep-marine systems. *Journal of the Geological Society*, *155*(2), 217–222. https://doi.org/10.1144/gsjgs.155.2.0217

Cattaneo, A., & Steel, R. J. (2003). Transgressive deposits: A review of their variability. *Earth-Science Reviews*, *62*(3–4), 187–228. https://doi.org/10.1016/S0012-8252(02)00134-4

Catuneanu, O. (2019). Model-independent sequence stratigraphy. *Earth-Science Reviews*, *188*, 312–388. https://doi.org/10.1016/j.earscirev.2018.09.017

Fagherazzi, S., & Overeem, I. (2007). Models of deltaic and inner continental shelf landform evolution. *Annual Review of Earth and Planetary Sciences*, *35*(1), 685–715. https://doi.org/10.1146/annurev.earth.35.031306.140128

Helland-Hansen, W., & Hampson, G. J. (2009). Trajectory analysis: Concepts and applications. *Basin Research*, *21*(5), 454–483. https://doi.org/10.1111/j.1365-2117.2009.00425.x

Helland-Hansen, W., Steel, R. J., & Sømme, T. O. (2012). Shelf genesis revisited. *Journal of Sedimentary Research*, *82*(3), 133–148. https://doi.org/10.2110/jsr.2012.15

Iwasaki, T., & Parker, G. (2020). The role of saltwater and waves in continental shelf formation with seaward migrating clinoform. *Proceedings of the National Academy of Sciences*, *117*(3), 1266–1273. https://doi.org/10.1073/pnas.1909572117

Maia, R. M. C., Reis, A. T., Alves, E. C., Silva, C. G., Guerra, J. V., Gorini, C., et al. (2010). Architecture and stratigraphic framework of shelf sedimentary systems off Rio de Janeiro State, northern Santos Basin—Brazil. *Brazilian Journal of Oceanography*, *58*(spe1), 15–29. https://doi.org/10.1590/s1679-87592010000500003

Muto, T. (2001). Shoreline autoretreat substantiated in flume experiments. *Journal of Sedimentary Research*, *71*(2), 246–254. https://doi.org/10.1306/091400710246

Muto, T., & Wang, J. (2024). Autogenic shrinkage and channel destabilization of an overexpanded downstream alluvial system under steady rise of relative sea level: An experimental study. *Earth and Planetary Science Letters*, *637*, 118722. https://doi.org/10.1016/j.epsl.2024.118722

Nittrouer, C. A., & Wright, L. D. (1994). Transport of particles across continental shelves. *Reviews of Geophysics*, *32*(1), 85–113. https://doi.org/10.1029/93RG02603

Patruno, S., Hampson, G. J., & Jackson, C. A. (2015). Quantitative characterisation of deltaic and subaqueous clinoforms. *Earth-Science Reviews*, *142*, 79–119. https://doi.org/10.1016/j.earscirev.2015.01.004

Patruno, S., & Helland-Hansen, W. (2018). Clinoforms and clinoform systems: Review and dynamic classification scheme for shorelines, subaqueous deltas, shelf edges and continental margins. *Earth-Science Reviews*, *185*, 202–233. https://doi.org/10.1016/j.earscirev.2018.05.016

Reis, A. T., Maia, R. M. C., Silva, C. G., Rabineau, M., Guerra, J. V., Gorini, C., et al. (2013). Origin of step-like and lobate seafloor features along the continental shelf off Rio de Janeiro State, Santos basin-Brazil. *Geomorphology*, *203*, 25–45. https://doi.org/10.1016/j.geomorph.2013.04.037

Ryan, W. B. F., Carbotte, S. M., Coplan, J. O., O'Hara, S., Melkonian, A., Arko, R., et al. (2009). Global multi-resolution topography synthesis. *Geochemistry, Geophysics, Geosystems*, *10*(3), Q03014. https://doi.org/10.1029/2008GC002332

Swift, D. J. P., & Thorne, J. A. (1992). Sedimentation on continental margins, I: A general model for shelf sedimentation. In D. J. P. Swift, G. F. Oertel, R. W. Tillman, & J. A. Thorne (Eds.), *Shelf sand and sandstone bodies: Geometry, facies and sequence stratigraphy, Special Publication of the International Association of Sedimentologists* (No. 14, pp. 1–31). Blackwell Scientific Publications. https://doi.org/10.1002/9781444303933.ch1

Tomer, A., Muto, T., & Kim, W. (2011). Autogenic hiatus in fluviodeltaic successions: Geometrical modeling and physical experiments. *Journal of Sedimentary Research*, *81*(3), 207–217. https://doi.org/10.2110/jsr.2011.19

Törnqvist, T. E., Wortman, S. R., Mateo, Z. R. P., Milne, G. A., & Swenson, J. B. (2006). Did the last sea level lowstand always lead to cross-shelf valley formation and source-to-sink sediment flux? *Journal of Geophysical Research*, *111*(F4), F04002. https://doi.org/10.1029/2005JF000425

Tozer, B., & Sandwell, D. T. (2019). Tozer et al., (2019) SRTM15+ GPlates project [Dataset]. *figshare*. https://doi.org/10.6084/m9.figshare.7973792.v1

Tozer, B., Sandwell, D. T., Smith, W. H. F., Olson, C., Beale, J. R., & Wessel, P. (2019). Global bathymetry and topography at 15 arc Sec: SRTM15+. *Earth and Space Science*, *6*(10), 1847–1864. https://doi.org/10.1029/2019EA000658

Walsh, J. J. (1988). *On the nature of continental shelves*. Academic Press.

Wang, J., & Muto, T. (2021). Autostratigraphic modelling of the growth of alluvial-shelf systems during steady base-level cycles: Two-dimensional tank experiments. *Sedimentology*, *68*(1), 135–167. https://doi.org/10.1111/sed.12789

Wang, J., & Muto, T. (2024). The intrinsic rarity of equilibrium response in stratigraphic processes. *Geosystems and Geoenvironment*, *3*(3), 100281. https://doi.org/10.1016/j.geogeo.2024.100281

Wang, J., & Muto, T. (2025). Shelf profile [Dataset]. *Zenodo*. https://doi.org/10.5281/zenodo.15702252

Wang, J., Tamura, T., & Muto, T. (2019). Construction and destruction of an autogenic grade system: The late Holocene Mekong River delta, Vietnam. *Geology*, *47*(7), 669–672. https://doi.org/10.1130/G45872.1

Wu, C., Nittrouer, J. A., Muto, T., Naito, K., & Parker, G. (2020). Morphodynamic equilibrium of lowland river systems during autoretreat. *Geology*, *48*(11), 1062–1066. https://doi.org/10.1130/G47556.1